◆ Human Brain Mapping 36:1–15 (2015) ◆

Evidence that Neurovascular Coupling Underlying the BOLD Effect Increases with Age During Childhood

Vincent J. Schmithorst,[1]* Jennifer Vannest,[1] Gregory Lee,[1] Luis Hernandez-Garcia,[2] Elena Plante,[3] Akila Rajagopal,[1] Scott K. Holland,[1] and The CMIND Authorship Consortium

[1]*Pediatric Neuroimaging Research Consortium, Department of Radiology, Cincinnati Children's Hospital Medical Center, Cincinnati, Ohio*
[2]*Department of Radiology, University of Michigan, Ann Arbor, Michigan*
[3]*Department of Speech, Language, and Hearing Sciences, University of Arizona, Tucson, Arizona*

Abstract: Functional MRI using blood–oxygen-level-dependent (BOLD) imaging has provided unprecedented insights into the maturation of the human brain. Task-based fMRI studies have shown BOLD signal increases with age during development (ages 5–18) for many cognitive domains such as language and executive function, while functional connectivity (resting-state) fMRI studies investigating regionally synchronous BOLD fluctuations have revealed a developing functional organization of the brain from a local into a more distributed architecture. However, interpretation of these results is confounded by the fact that the BOLD signal is directly related to blood oxygenation driven by changes in blood flow and only indirectly related to neuronal activity, and may thus be affected by changing neuronal–vascular coupling. BOLD signal and cerebral blood flow (CBF) were measured simultaneously in a cohort of 113 typically developing awake participants ages 3–18 performing a narrative comprehension task. Using a novel voxelwise wild bootstrap analysis technique, an increased ratio of BOLD signal to relative CBF signal change with age (indicative of increased neuronal–vascular coupling) was seen in the middle temporal gyri and the left inferior frontal gyrus. Additionally, evidence of decreased relative oxygen metabolism (indicative of decreased neuronal activity) with age was found in the same regions. These findings raise concern that results of developmental BOLD studies cannot be unambiguously attributed to neuronal activity. Astrocytes and astrocytic processes may significantly affect the maturing functional architecture of the brain, consistent with recent research demonstrating a key role for astrocytes in mediating increased CBF following neuronal activity and for astrocyte processes in modulating synaptic connectivity. *Hum Brain Mapp 36:1–15, 2015.* © 2014 Wiley Periodicals, Inc.

Contract grant sponsor: National Institutes of Health Pediatric Neuroimaging Functional Research Network; Contract grant number: HHSN275200900018C

Vincent J. Schmithorst is currently at Pediatric Imaging Research Center, Dept. of Radiology, Children's Hospital of Pittsburgh of UPMC, 4401 Penn Ave., Pittsburgh, PA 15224

*Correspondence to: Vincent J. Schmithorst. Pediatric Neuroimaging Research Consortium, Dept. of Radiology Cincinnati Children's Hospital Medical Center, 3333 Burnet Ave. Cincinnati, OH 45229, USA. E-mail: Vincent.Schmithorst@chp.edu

Received for publication 9 May 2014; Revised 30 July 2014; Accepted 3 August 2014.

DOI: 10.1002/hbm.22608
Published online 19 August 2014 in Wiley Online Library (wileyonlinelibrary.com).

© 2014 Wiley Periodicals, Inc.

Key words: functional MRI; children; neuronal–vascular coupling; language processing; developmental studies

INTRODUCTION

Functional magnetic resonance imaging (fMRI) is a noninvasive modality which has yielded an unprecedented amount of information pertaining to brain development in infants and children, and even holds the promise of aiding in diagnosis and treatment of neurodevelopmental disorders. Reflecting the developing architecture of the brain, regional task-based fMRI signal increases with age during the developmental period (ages 5–18) have been seen in a large variety of tasks, including receptive language [Szaflarski et al., 2012], expressive language [Szaflarski et al., 2006], motor function [Schapiro et al., 2004], and executive function [Luna et al., 2010]. Functional connectivity MRI (fcMRI; also called "resting-state" fMRI), which is fMRI data collected without stimulation by a specific task, measures regionally correlated fluctuations of fMRI signal thought to be related to spontaneous neural fluctuations. FcMRI studies have shown increases in global and local functional brain network connectivity [Dosenbach et al., 2010], with the remarkable finding that the age of a subject (between 7 and 30 years) may be predicted by fcMRI results as the brain's functional organization shifts from a more local to a more distributed architecture with age.

However, the precise physiological correlates of these results are unclear since the fMRI signal measured in these experiments is only an indirect measure of neuronal activity. The blood–oxygen-level-dependent (BOLD) signal measured in fMRI experiments is caused by changes in the amount of venous deoxyhemoglobin (which is paramagnetic and causes MRI signal attenuation) resulting from the oxidative metabolic demand due to neuronal activity. Increased metabolic demand (for instance, the result of a change between a "baseline" and an "active" condition in a task-based fMRI experiment), causes hyperemia (increased cerebral blood flow [CBF]), which results in lower levels of venous deoxyhemoglobin and a positive BOLD signal contrast. Since the BOLD signal is a function of the amount of hyperemia, population differences in BOLD signal magnitude can theoretically result from differences in neuronal–vascular coupling (the relationship between increased task-based neuronal metabolic demand and hyperemia) instead of differences in neuronal activity [Davis et al., 1998], while population differences in BOLD signal correlations (such as used in fcMRI experiments) can theoretically result from regional differences in neuronal–vascular coupling instead of differences in functional topology. In addition to possible misinterpretation of BOLD signal differences, another consideration is that some developmental changes in brain function may not be detectable via BOLD imaging alone if changes in neuronal activity with age are counterbalanced by opposite changes in neuronal–vascular coupling.

Whether potential age-related differences in neuronal–vascular coupling in fact represent a significant confound for developmental fMRI studies has been much debated in the literature. Based on results from animal studies involving mechanisms known to contribute to neuronal–vascular coupling and known to change over development in animals, Harris et al. [2011] hypothesize that "...developmental changes in neurovascular coupling are likely to contribute to observed developmental changes in BOLD signals" (p. 211). Conversely, Church et al. [2010] argue that many results seen in prior developmental fMRI studies, such as different tasks resulting in different relationships of activity between children and adults within the same region, cannot be explained by differences in neuronal–vascular coupling. In adult studies, wide intersubject variability in neuronal–vascular coupling has been seen [Davis et al., 1998; Hoge et al., 1999; Kastrup et al., 2002; Kim et al., 1999; Uludag et al., 2004]. However, there is as yet a paucity of in vivo data available in children.

Therefore, to directly investigate this question, we used a double excitation MR imaging method specially designed to concurrently acquire both a BOLD-weighted image and arterial spin-labeled (ASL) image of relative CBF change from the same volume [Schmithorst et al., 2014]. Using this method, we acquired concurrent ASL and BOLD images during performance of a task-based fMRI paradigm involving narrative comprehension in a cohort of 113 normally developing children ages 3–18. The ASL technique "labels" blood entering the brain through the carotid arteries, and therefore, enables the noninvasive measurement of CBF. This technique is suitable for use in a healthy pediatric population [Holland et al., 2014], whereas more invasive techniques for measuring CBF (such as positron emission tomography [PET], or dynamic susceptibility contrast MRI, involving a contrast agent) are unacceptable for use in research in healthy children.

MATERIALS AND METHODS

Participants

Data was successfully acquired from 113 participants ages 3 years 1 month to 18 years 9 months (58 females; see Table I for complete age and gender breakdown). All children were right-handed native speakers of English with no history of neurological or psychiatric disease in the children or in first-degree relatives. The study was

TABLE I. Age and gender breakdown of the study participants

Age (years:months)	*N* (boys)	*N* (girls)
3:1–5:11	8	11
6:0–8:11	21	15
9:0–11:11	8	8
12:0–14:11	13	11
15:0–18:9	7	9

approved by the Institutional Review Board at Cincinnati Children's Hospital Medical Center; informed consent and assent (where appropriate) were obtained from a parent/guardian and the participant.

Neurocognitive Data

A standardized neuropsychological assessment including age appropriate Wechsler IQ scales: Wechsler Preschool & Primary Scale of Intelligence, Third Edition (WPPSI-III, ages 2:6–5); Wechsler Intelligence Scale for Children, Fourth Edition (WISC-IV, ages 6–16) Wechsler Adult Intelligence Scale, Fourth Edition (WAIS-IV, ages 17 and 18) was completed by 104 out of the 113 children. Results were in the normal range (mean IQ $\pm$ std. = 107 $\pm$ 14.6); there was no correlation with age ($R = -0.06$, $P > 0.5$) and no significant difference between boys and girls ($T = 0.016$, $P > 0.9$).

Scanning Procedures for Very Young Participants

In participants of age 5 years and under, additional preparation time was allowed at each session to acclimate the child to the scanner environment. During this time, study personnel used a step-by-step approach to introduce the equipment, including the headphones and microphone for in-scanner communication. Young children were given stickers as tangible reinforcers frequently during the acclimation process. Based on these strategies, only two young children who were recruited for this session were unable to enter the scanner during the visit. One additional child participated but exited the scanner before the narrative comprehension task.

fMRI Task Paradigm

Participants completed a functional MRI scanning session during which they performed a narrative comprehension task, comprised of five different stories, each 1 min in duration, designed by a speech–language pathologist to be appropriate for young children and read by an adult female speaker. Stories were presented in a 64-s alternating block design. During the control blocks, broadband noise in the frequency range of speech was presented in a gradual sweep across frequencies (500–4,000 Hz). The duration of each sweep varies from 0.5 to 4 s. This comparison between naturalistic speech and nonspeech auditory processing engages multiple aspects of language processing while controlling for sublexical auditory stimulation. Five 64-s blocks of stories and five 64-s control blocks of broadband noise were alternated for a total scan time of 10 min 40 s. All children were awake during the entire duration of the scan.

Combined Whole-Brain Functional ASL/BOLD Gradient-Echo EPI Acquisitions

MRI data was obtained using a Philips 3T Achieva system and a 32-channel head coil. For the combined whole-brain functional ASL/BOLD acquisitions, a double-excitation approach was used, determined both theoretically and empirically to be more optimal as compared to double-echo acquisitions or other methods [Schmithorst et al., 2014]. Acquisition parameters were: repetition time (TR) = 4,000 ms, (echo time) TE1 = 11 ms, TE2 = 35 ms, matrix = 64 $\times$ 64, field of view (FOV) = 25.6 $\times$ 25.6 cm^2, slice thickness = 5 mm, 25 slices acquired covering the whole brain. Parameters for the pseudocontinuous spin-labeling were: labeling duration = 1,500 ms, postlabel delay = 700 ms, mean $B1 = 1.0$ μT, mean gradient = 1.0 mT/m during tag periods (mean gradient = 0 during control), max gradient = 6 mT/m, pulse duration = 500 μs, time between pulses = 1.5 ms. The postlabel delay (700 ms) is shorter than those typically used for nonfunctional ASL acquisitions used to estimate absolute CBF. This approach was recommended by Gonzalez-At et al. [2000], when only the relative CBF change is of interest, as the shorter postlabel delay enhances the CNR. Similar values have been used by previous studies [Aguirre et al., 2002; Fernandez-Seara et al., 2009; Lim et al., 2010]. We also note that, even for the first (bottom-most) slices acquired, the total labeling plus postdelay time (2,200 ms) is sufficient to allow at least a significant proportion of the labeled spins to reach the capillaries. This proportion will increase significantly for later-acquired slices since the effective postdelay time is longer due to the time necessary to acquire the earlier slices (the total time needed to acquire all 25 slices is approximately 500 ms, leading to an effective postlabel delay of 1,200 ms for the top-most slices and approximately 1,000 ms for the middle slices).

First-Level Analysis

First-level fMRI data processing was performed using FMRI Expert Analysis Tool (FEAT) Version 6.0, part of FMRIB's Software Library (FSL, www.fmrib.ox.ac.uk/fsl), involving motion correction, spatial smoothing, coregistration to a study-specific template, and a general linear model (GLM) with autocorrelation correction to compute BOLD and ASL activation. Prior to first-level analysis,

datasets were discarded if gross motion artifacts were present via visual inspection.

Independent motion correction of the ASL and BOLD timeseries (to a common reference frame) was performed using MCFLIRT [Jenkinson et al., 2002]. In an initial run, the central timepoint was used as the reference frame. Based on the derived motion parameters, the timepoint with the minimal displacement from the average position of the brain over the timeseries was determined. Motion correction was then restarted, using this minimal displacement timepoint as the reference frame. Following motion correction, spatial smoothing using a Gaussian kernel of FWHM 8 mm and highpass temporal filtering (Gaussian-weighted least-squares straight line fitting, with $\sigma = 64$ s) were applied. Grand-mean intensity normalization by a single multiplicative factor was applied to each 4D dataset.

A study specific T1-weighted template encompassing the age range in our study was created using a template creation script (buildtemplateparallel.sh) available as part of Advanced Normalization Tools (ANTs, stnava.github.io/ANTs/). One hundred thirty-five subjects (61 male, 87 female) between the ages of 4 and 18 years were used to form the template. Prior to the template creation, the T1-weighted anatomical images were bias corrected using the N4ITK algorithm [Tustison et al., 2010]; nonbrain removal was then performed using BET [Smith, 2002]. A nonlinear warping of the resulting template to 2-mm MNI standard space was then computed using symmetric diffeomorphic image normalization (SyN) [Avants et al., 2008], as implemented in ANTs.

To normalize the functional datasets to the template, the timeseries-averaged CBF map (control-tag) was computed from the motion corrected ASL data. The CBF image has high GM/WM contrast due to the large perfusion difference in these tissue types. A linear, affine boundary-based registration [Greve and Fischl, 2009] as implemented in FLIRT (FMRIB's Linear Image Registration Tool) [Jenkinson and Smith, 2001; Jenkinson et al., 2002] was used for transformation of each subject's mean CBF map to anatomical space. This affine transformation computed from the mean CBF-weighted image was then kept for later use in transforming ASL or BOLD functional images and statistic maps to standard space.

Timeseries statistical analysis was performed using FILM with local autocorrelation correction [Woolrich et al., 2001]. The following regressors were used in a GLM design matrix for both BOLD and ASL timeseries analysis: (1) A BOLD task regressor corresponding to five repetitions of a 64 s ON, 64 s OFF square wave convolved with a double-gamma hemodynamic response function. (2) The temporal derivative of the BOLD task regressor. (3) An ASL baseline CBF signal regressor (alternating values of 0.5, −0.5 for control, tag, respectively). The BOLD-related regressor is included in the ASL design matrix to model residual BOLD signal at TE = 11.5 ms. Similarly the tag/control regressor is present during BOLD data analysis to model any small, residual effects of the ASL tagging process on the BOLD timeseries. ASL timeseries analysis was performed on unsubtracted data following the approach of [Mumford et al., 2006]. For the ASL timeseries analysis, there was a fourth regressor corresponding to CBF-based task-related signal change. This regressor is the product of the BOLD task regressor and the CBF baseline signal regressors (after mean centering of each). Six motion parameters (3 translations, 3 rotations) derived during timeseries coregistration were used as nuisance regressors. Additionally, a subject-dependent number of individual nuisance regressors for removing outlier timepoints were created using the fsl_motion_outliers tool, employing the "refrms" metric. This metric applies a threshold on the root-mean-squared intensity difference between a given volume and a reference volume to identify intensity outliers. The threshold used was the standard boxplot outlier threshold, thresh = p75 + 1.5 × (p75 − p25), where p25 and p75 are the 25th and 75th percentiles for the RMS differences, respectively. This is closely related to the DVARS metric recently proposed [Power et al., 2012].

Second-Level Analysis

Second-level analysis was performed on a voxelwise basis using routines written in IDL (Exelis, Boulder, CO), using the raw % BOLD and % CBF signal changes as the independent variables. One-sample *T*-tests were performed on the ASL and BOLD data to qualitatively compare the sensitivity of the techniques. Results were thresholded at $T > 4.5$ and spatial extent threshold of 100 voxels; this corresponded to a family-wise error (FWE)-corrected $P < 0.01$ using the Monte Carlo method (described in detail below for the investigation of BOLD signal changes with age).

Subsequent analyses (described below) were restricted to voxels with significant ($T > 2.25$, $P < 0.03$) activation for ASL, as the relevant parameters we wish to investigate (described in detail below) cannot be estimated if $\Delta CBF = 0$. The threshold chosen ($T > 2.25$) was slightly stricter than a nominal $P < 0.05$, as it was found that a looser threshold led to nonrobustness of the voxelwise bootstrap used (described below), as in some bootstrap iterations the fit of ΔCBF as a function of participant age could dip below zero.

Analysis 1: Changes in the Ratio of BOLD to Relative CBF Change (rBOLDCBF) with Age

The rationale for this analysis is that the BOLD signal can be modeled as a linear function of the relative CBF change between baseline and active conditions:

$$\mathrm{BOLD} = M(\beta - \alpha - \beta n^{-1})\frac{\Delta \mathrm{CBF}}{\mathrm{CBF}} \quad (1)$$

using a first-order Taylor expansion (see Appendix for derivation) of the empirically validated Davis model

[Davis et al., 1998; Griffeth and Buxton, 2011], where M is the theoretical maximum BOLD signal (related to baseline deoxyhemoglobin content), β is a parameter relating deoxyhemoglobin concentration to MRI signal (a function of blood vessel geometry), α is a parameter (known as Grubb's constant) relating blood volume change to CBF change, n is the neuralglial–vascular coupling constant (defined below), CBF_0 is the blood flow in the baseline condition, CBF is the blood flow in the active condition, $\Delta CBF = CBF - CBF_0$.

The neuralglial–vascular coupling constant n is of primary interest in the current analysis and is defined as:

$$n = \frac{\frac{\Delta CBF}{CBF_0}}{\frac{\Delta CMRO_2}{CMRO_{20}}} \quad (2)$$

where $CMRO_{20}$ is the metabolic rate of oxygen in the baseline condition, $CMRO_2$ is the metabolic rate of oxygen in the active condition, $\Delta CMRO_2 = CMRO_2 - CMRO_{20}$. Assuming minimal changes in M or α with age during development (cf. Discussion section), from Eq. (1), we can infer age-related changes in n from age-related changes in rBOLDCBF without the need to estimate absolute values of either M or n. Diverging from typical nomenclature in the literature, we have renamed n the neuralglial–vascular coupling constant (instead of neurovascular coupling constant) since a significant portion, estimated at 15%–30%, of oxidative metabolism in the brain occurs in astrocytes and not neurons [Hertz et al., 2007]. n will be an accurate estimator of neurovascular coupling only if the ratio of neuronal oxygen metabolism to astrocytic oxygen metabolism does not change with task condition. (Implications for violation of this assumption are mentioned in the Discussion section.)

To find regions with significant age-related changes in rBOLDCBF, the calculated ΔCBF/CBF and BOLD values in each voxel were linearly fit to participant age. The fitted values were then used in Eq. (1) to generate estimates of the rate of change of rBOLDCBF coupling with participant age. Statistical significance was ascertained using a wild bootstrap (detailed below). This procedure is used in preference to a direct estimate of rBOLDCBF from Eq. (1) as noise in the CBF data results in very high errors in the estimate due to division by numbers close to zero. (We did not attempt higher-order models as the goal of this analysis was not to attempt to accurately map developmental trajectories, but only to test for the existence of age-related changes; linear models are typically used in standard GLM analyses of neuroimaging data. Additionally, we were precluded from accurate modeling of nonlinear fits due to the amount of noise in the CBF data.)

Analysis 2: Changes in Neuronal Activity (as indexed by $CMRO_2$) with Age

The rationale for this analysis is that we also wish to understand developmental changes in the brain's functional organization (above and beyond physiologic factors). Therefore, we used a similar voxelwise procedure to investigate age-related changes in neuronal activity (indexed by $CMRO_2$) distinct from changes in hyperemia. We use the following expression for the BOLD signal (see Appendix for derivation):

$$BOLD = M(\beta - \alpha)\frac{\Delta CBF}{CBF} - M\beta\frac{\Delta CMRO_2}{CMRO_{20}}\left(1 - \frac{\Delta CBF}{CBF}\right) \quad (3)$$

However, the presence of the intercept term here, however, means that we cannot simply compute a ratio (unlike Analysis 1) and we need to estimate values for M, α, and β in order to investigate changes in $\Delta CMRO_2/CMRO_{20}$ with participant age. We used literature values of $\beta = 1.3$ and $\alpha = 0.2$ [Chen and Pike, 2009]. We note that an estimate of M at each voxel is available from Eq. (1) using the participant-wise averages of BOLD and ΔCBF/CBF, if the average n were also known. Therefore, we assumed a participant-wise average value of $n = 2.0$ as found in previous studies [Hoge et al., 1999]. (Note that while our analysis assumes a value for the participant-wise average n, it does not assume a fixed n across participants.) Using these estimates of M [from Eq. (1)], the linearly fitted ΔCBF/CBF and BOLD values from Analysis 1 were used in Eq. (3) to generate estimates of the rate of change of $\Delta CMRO_2/CMRO_{20}$ with participant age. Statistical significance was ascertained using a wild bootstrap (detailed below).

Statistical Significance Assessed Using Novel Voxelwise Wild Bootstrap

For each analysis, T-scores (parameter estimates and their standard errors) for each voxel were computed using a wild bootstrap procedure (250 iterations). Statistical significance (FWE) was assessed using the same wild bootstrap but with the null hypothesis enforced to create "noise" maps [Ledberg et al., 1998]. To maintain the residual spatial autocorrelation and not bias the estimate of significance, the sign multiplying each residual was kept constant over the whole brain for each bootstrap iteration. For a T threshold of 2.75 and a spatial extent threshold of 200 voxels, the wild bootstrap procedure revealed these thresholds to correspond with a FWE-corrected $P < 0.05$.

Analysis 3: Investigating Changes in BOLD Signal with Age

For comparison with prior studies, a standard GLM was used to find regions with a significant correlation of BOLD signal with participant age. The number of degrees of freedom from the first-level analysis was incorporated into the design matrix as a covariate. Statistical significance was assessed via the Monte Carlo method of Ledberg et al. [1998] with estimates of spatial autocorrelation taken from the fit residuals. A T threshold of 2.75 and spatial extent

threshold of 150 voxels corresponded to a FWE-corrected $P < 0.05$ (the spatial extent threshold is slightly smaller than for the previous analyses as the intrinsic spatial smoothness is lower since only BOLD data and not combined ASL–BOLD data was used in the analysis).

Post hoc Region of Interest Analyses

ROI analyses were performed for each region found in Analyses 2 and 3 to investigate, which factors are driving the age-related changes seen in relative $CMRO_2$ and BOLD signal, respectively. For each participant, BOLD and CBF values were averaged over the ROI. M was estimated in the same manner as Analysis 2 (assuming participant-wise average $n = 2.0$; note, however, that assuming a participant-wise average value of n does not preclude age-related changes in n). $\Delta CMRO_2/CMRO_{20}$ was then directly calculated from Eq. (3) (the higher SNR available from voxel averaging makes this procedure feasible). Since noise present in the $\Delta CMRO_2/CMRO_{20}$ data still precluded a direct calculation of n, BOLD, $\Delta CBF/CBF_0$, and $\Delta CMRO_2/CMRO_{20}$ were linearly fit to participant age. The fitted values were then used to compute median and 95% confidence limits on n as a function of participant age [from Eqs. (1), (2), and (3)] using a bootstrap (resampling with replacement; 1,000 iterations). (This analysis is circular only to the extent that absolute values of $\Delta CMRO_2$ and n are computed using our assumed participant wise $n = 2.0$, and our results should not be taken as indicative of absolute values of these parameters; however, our analysis is not circular insofar as age-related changes in relative $\Delta CMRO_2$ and n are our variables of interest.)

RESULTS

We present results from the Pediatric Functional Neuroimaging Research Network database (C-MIND). All data (including functional ASL/BOLD, baseline CBF measurements, and whole-brain T1-anatomical scans) is freely available online from the C-MIND database in either raw or postprocessed format (https://research.cchmc.org/c-mind/), as well as demographic, neuropsychological, and neurobehavioral data. In the dataset presented here, participants performed a "child-friendly" task-based fMRI paradigm (narrative comprehension) previously used to study the neural circuitry of child language development [Holland et al., 2007]. Data was acquired using a combined ASL/BOLD data acquisition technique optimized for whole-brain acquisitions [Schmithorst et al., 2014]. BOLD data from this task has shown increases in signal with age [Szaflarski et al., 2012] despite the fact that narrative comprehension is an early-developing language skill, raising the question of whether the increased BOLD signal may have a different etiology than increased neuronal activity. A qualitative comparison of the two techniques (Figs. 1 and 2) reveals similar sensitivity for the two techniques, with perhaps somewhat greater sensitivity overall for BOLD: while both techniques robustly detected activation in the middle and superior temporal gyri in both hemispheres, the BOLD technique additionally found activation in the medial frontal gyrus and inferior frontal gyrus in the left hemisphere. Conversely, activation in the left cerebellum was only detected with ASL.

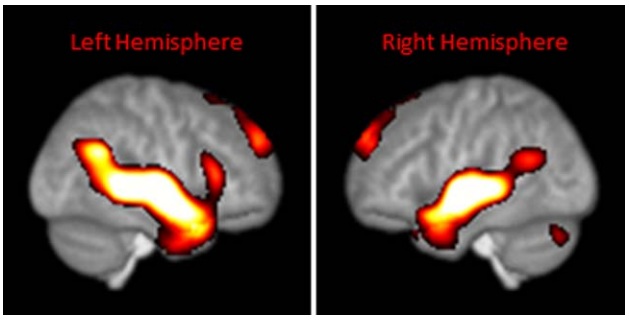

Figure 1.
Map showing regions of significant functional BOLD activation during performance of a narrative comprehension task by 113 participants of age 3–18 years. [Color figure can be viewed in the online issue, which is available at wileyonlinelibrary.com.]

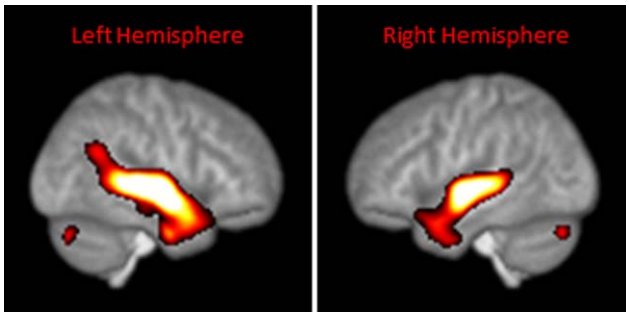

Figure 2.
Map showing regions of significant functional ASL activation during performance of a narrative comprehension task by 113 participants of age 3–18 years. [Color figure can be viewed in the online issue, which is available at wileyonlinelibrary.com.]

For Analysis 1, we used a novel voxelwise bootstrap analysis procedure (which properly accounts for multiple comparisons in assessment of statistical significance) to find regions with changing rBOLDCBF coupling with age, representative of changing n with age (analysis was restricted to regions with significant group ASL activation). Increases in n with age were seen for most regions activated during the task, including the middle temporal gyri bilaterally, and in the left inferior frontal gyrus (BA 47) as illustrated in Figure 3.

These findings of increasing n with age observed in Analysis 1 allow us to infer developmental changes in neurovascular physiology. To investigate possible changes in brain function, we used the same voxelwise wild

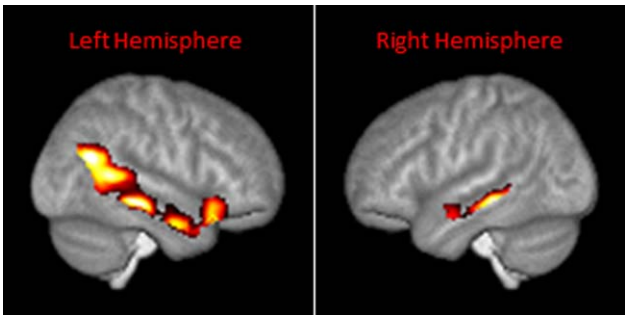

Figure 3.
Map showing regions of significant change in the ratio of BOLD signal to ΔCBF/CBF [rBOLDCBF; a marker for neuralglial–vascular coupling (n)] as a function of age during performance of a narrative comprehension task by 113 participants of age 3–18 years (Analysis 1). Regions with increasing rBOLDCBF as a function of age are indicated by warm colors. [Color figure can be viewed in the online issue, which is available at wileyonlinelibrary.com.]

bootstrap procedure to find regions with changing relative $\Delta CMRO_2$ with age (representative of neuronal activity). Most of the regions found to exhibit a positive relation between age and neuralglial–vascular coupling as shown in Figure 1 also displayed a negative relation between age and relative $\Delta CMRO_2$ as illustrated in Figure 4. Results did not depend significantly on the choice of average n (data not shown).

Post hoc analyses examining BOLD and CBF changes with age were performed on the regions with relative $CMRO_2$ decreases with age found in Analysis 2 (averaging the BOLD and CBF values for each participant across the region of interest). Figure 5 displays the result of this analysis for the left middle temporal gyrus, revealing that n increased with participant age ($P < 0.025$, via bootstrap). The combination of decreasing relative $\Delta CMRO_2$ and increasing n results in the BOLD signal remaining fairly constant ($R = -0.05$, $P > 0.5$), but the relative CBF decreasing with participant age ($R = -0.29$, $P < 0.01$).

Results from Analysis 1 provide strong evidence that neurovascular coupling increases with age—this physiologic change may underlie age-related increases in BOLD frequently observed in previous studies, while neuronal activity in the same regions may be stable or even decrease across development. To investigate this, in Analysis 3, we performed a voxelwise analysis on the BOLD data only, testing for regions with increased BOLD signal with age. We found increased BOLD signal with age only in a specific subregion of the middle temporal gyrus in the left hemisphere, shown in Figure 6.

A similar post hoc ROI analysis was performed on the subregion with BOLD signal increases with age, revealing no significant age-related change in relative CBF ($R = -0.04$, $P > 0.5$). Further analysis revealed (Fig. 7) that the BOLD signal increase is driven by a significant age-related increase in n ($P < 0.05$, via bootstrap) with no significant change seen in relative $\Delta CMRO_2$ ($R = -0.1$, $P > 0.3$). (Note that in the adolescent age range from age 12 to 18 years, the variability on our estimates of n increases dramatically as a result of the dependence of this term on the change in $\Delta CMRO_2$ in the denominator in Eq. (2), which dramatically decreases with age).

DISCUSSION

An increasing number of fMRI studies in the published literature discuss changes in BOLD signal with age in children as a surrogate marker for cognitive brain development. The current analysis goes beyond examination of BOLD changes alone to investigate developmental changes in the relation between neuronal activity, CBF, and BOLD signal. This is an important area of research since little is known about how neuronal–vascular coupling may change with development during childhood. Our findings have implications for interpretation of developmental fMRI studies and raise questions concerning the underlying mechanism that couples neuronal activity reflected in $CMRO_2$ to CBF in the developing brain.

We found evidence of age-related changes in n in many of the regions activated during the language stimulation task, including the middle temporal gyrus and left inferior frontal gyrus (BA 47), and most of these regions also displayed evidence of decreased relative $\Delta CMRO_2$. However, increased BOLD signal was only found in a small subregion of the left middle temporal gyrus, agreeing with previous reports [Holland et al., 2007; Szaflarski et al., 2012].

These results indicate that important facets of brain development may not be detectable via BOLD imaging if changes in neuronal–vascular coupling are opposite to

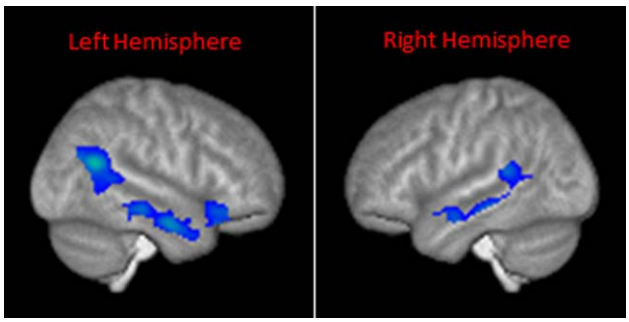

Figure 4.
Map showing regions of significant change in relative cerebral metabolic rate of oxygen ($CMRO_2$; a marker for neuronal activity) as a function of age during performance of a narrative comprehension task by 113 participants of age 3–18 years (Analysis 2). Regions where $\Delta CMRO_2/CMRO_{20}$ decreases significantly with age are indicated by cold colors. [Color figure can be viewed in the online issue, which is available at wileyonlinelibrary.com.]

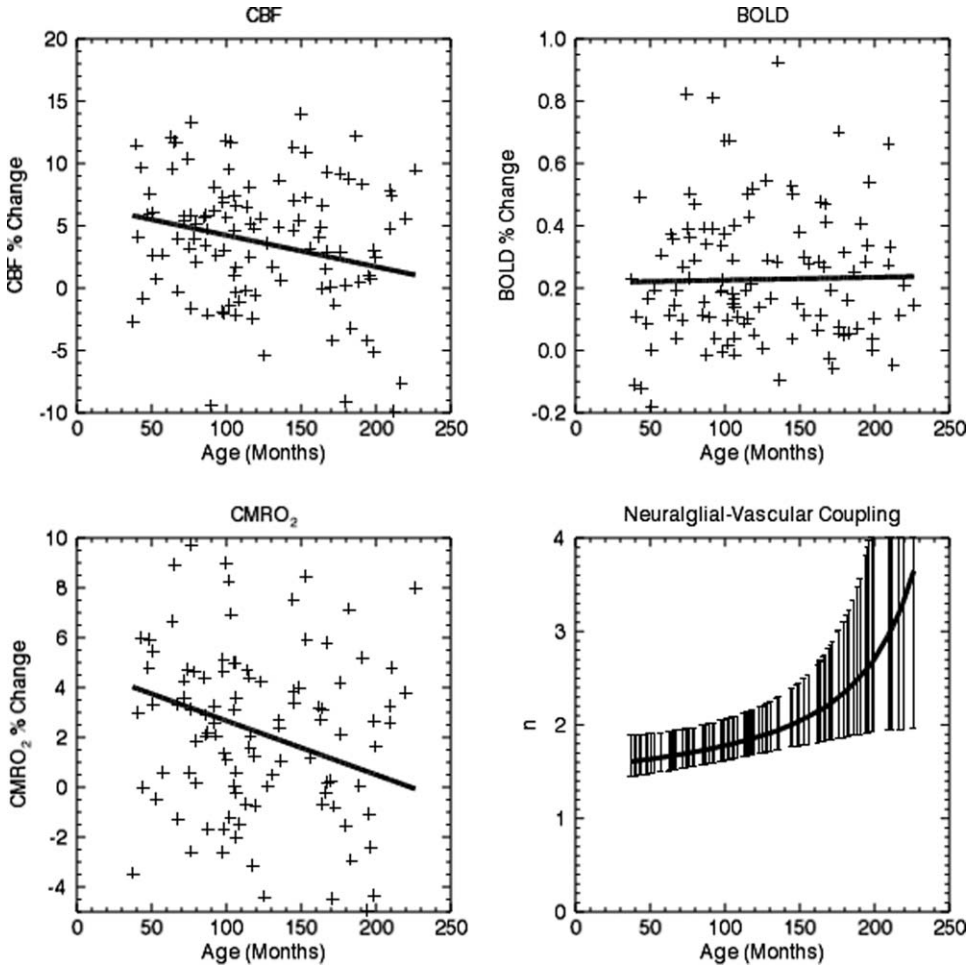

Figure 5.

Graphs of CBF % signal change (top left), and BOLD % signal change (top right) in the left middle temporal gyrus (highlighted in Figure 4) as a function of age during performance of a narrative comprehension task by 113 participants of age 3–18 years (solid lines are linear fits vs. participant age). Note CBF decreases with participant age while BOLD signal remains constant with age. This indicates decreasing relative $CMRO_2$ change with age (bottom left), and increasing *n* with age (bottom right). Values of *n* plotted are median (solid line) and 95% confidence intervals (error bars) obtained from bootstrapping (1,000 iterations, resampling with replacement) of a linear fit of participant age to CBF and $CMRO_2$. (Error bars are much larger at older ages due to the lower values of $CMRO_2$.)

changes in neuronal activity, as a decrease in relative $\Delta CMRO_2$ combined with increased *n* can result in decreasing relative ΔCBF and constant BOLD signal. Here we found, for an "early-developing" language task (narrative comprehension), evidence for widespread changes in neuronal activity, showing decreased activity in higher-order auditory association, semantic processing, and visual processing regions, likely associated with more efficient processing.

These findings also reveal a danger of misinterpreting developmental changes in BOLD signal as related to neuronal activity, whereas they may be instead be driven by changes in neuronal–vascular coupling. In several studies involving elderly populations, neuronal–vascular coupling has been identified as a significant confound, causing BOLD signal decreases in some regions for which neuronal activity was found to actually increase when controlled for the changes in coupling [Hutchison et al., 2013; Peiying et al., 2013]. The correlation of BOLD signal with age previously observed for this task was interpreted as greater neuronal activation [Szaflarski et al., 2012]. However, our results demonstrate that this result is instead driven by increased *n*. Interestingly, the increase in BOLD signal was found precisely in the subregion of the left middle temporal gyrus for which no decrease in relative $\Delta CMRO_2$ was found.

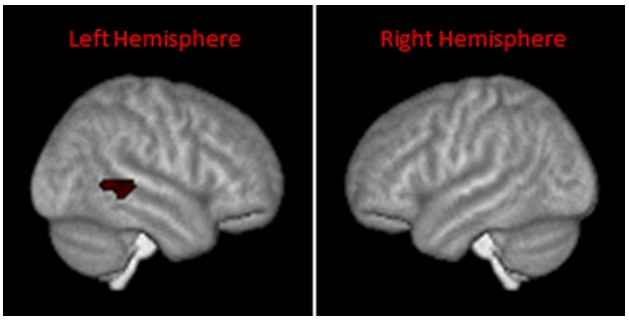

Figure 6.
Map of BOLD signal as a function of age during performance of a narrative comprehension task by 113 participants of age 3–18 years (Analysis 3). Regions with increasing BOLD signal with age are indicated by warm colors. [Color figure can be viewed in the online issue, which is available at wileyonlinelibrary.com.]

Our results, therefore, fail to support the blanket claim [Church et al., 2010] that "Developmental differences are not vascular" (p. 855). Nevertheless, we certainly also would not support the alternative blanket claim that "*All* developmental differences are vascular." The arguments raised to the contrary [Church et al., 2010, 2012] are reasonable and certainly merit further discussion. In a commentary on the review article [Harris et al., 2011] in which developmental changes in neuronal–vascular coupling are hypothesized to be a significant confound, Church et al. [2012] cite two main pieces of evidence against a significant contribution from neuronal–vascular coupling differences: (1) adult and child BOLD % signal change is not significantly different over most of the brain; and (2) observed differences are task specific and not task general. Regarding (1), our study also showed no difference in BOLD signal between older and younger children for most of the regions activated during the task. However, this was shown to not result from neuronal activity and neuronal–vascular coupling remaining constant with age, but rather the result of counteracting differences. Indeed, we do find it quite plausible that over development, as the brain becomes more efficient at performing various cognitive tasks, the amount of neural resources needed to perform those tasks will decrease. Stronger evidence is provided by (2), however, especially if different tasks produce opposite differences in BOLD signal (e.g., more BOLD signal in the older age group for one task, but less BOLD signal for another). It is possible, as commented by [Harris et al., 2011], that different inputs to a given region could have different developmental trajectories in the relation of vascular response to neuronal activity. We admittedly find this possibility rather far-fetched (although we note it could be investigated by task-based ASL/BOLD fMRI experiments similar to that performed in the present study), and we would indeed interpret this data as indicative of differing developmental trajectories in neuronal activity dependent on task. However, we note that from this conclusion we cannot infer differences in neuronal activity for any single task; but only that, if neuronal activity is unchanged for one task, there must be differences in the other. We would, therefore, modify the conclusion [Church et al., 2010] that "Such manipulations of activity should not be possible if the differences in brain activity over age were due to neurovascular effects" (p. 855) to read "Such manipulations of activity should not be possible if all differences in brain activity over age were due to neurovascular effects."

In addition to the two pieces of evidence cited above, additional pieces of evidence have also been put forth [Church et al., 2010]: (1) Regionally dependent increases and decreases in BOLD signal differences arise from performance of the same task; and (2) the location of group differences is task-dependent. While the data in (1) can be explained via regionally dependent changes in neuronal–vascular coupling, this is not sufficient to explain the data in (2), which we would again interpret as task-dependent differences in developmental trajectories of neuronal activation, but with the same difficulties in inferring conclusions about any single task as stated above. Thus, we would again modify the statement [Church et al., 2010] that "A developmental difference in neurovascular coupling cannot account for this array of observations." (p. 855) to read "Developmental differences in neurovascular coupling cannot account for this array of observations in toto, but they may account for some of the findings."

We note the same possibility of misinterpreting changes in BOLD signal is present in fcMRI studies, where correlations of spontaneous BOLD signal changes are measured, rather than comparisons between a task and baseline condition. Increased neuronal–vascular coupling in two brain regions will result in increased measured functional connectivity between those regions even with similar levels of synchronous neural activity because the correlation coefficient (full or partial) used as a metric of connection strength will increase with the BOLD signal strength. This confound may be of less concern when graph theory (see [Rubinov and Sporns, 2010] for a review) is used to characterize brain network topology, if statistical controls are applied for overall network cost (corresponding to overall connectivity). However, regional differences in neuronal–vascular coupling with development may also yield spurious differences in brain network topology.

The above confounds are likely to be more severe when BOLD fMRI is used to investigate neurocognitive or neurodevelopmental disorders. Such pathologies may further alter the development of neuronal–vascular coupling as well as synaptogenesis and overall brain architecture. Pathologies directly associated with hemoglobin or vascular pathology (e.g., sickle cell anemia, pediatric stroke) have obvious implications for measuring the BOLD response. The presence of sickle cell anemia has been associated with reduced BOLD signal, even when a number of parameters that likely impact the neural–vascular coupling are statistically controlled [Zou et al., 2011]. Less obvious

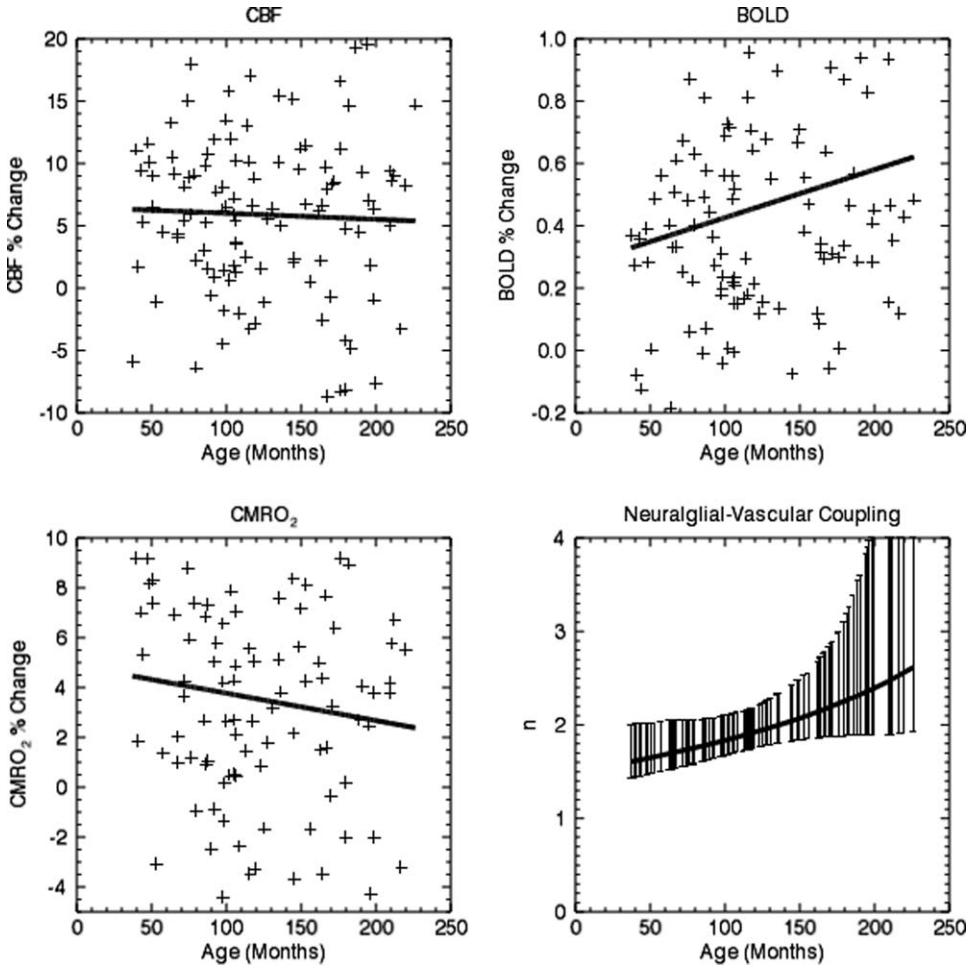

Figure 7.

Graphs of CBF % signal change (top left), and BOLD % signal change (top right) in a subregion of the left middle temporal gyrus (cf. Figure 6) as a function of age during performance of a narrative comprehension task by 113 participants of age 3–18 years (solid lines are linear fits of signal change vs. participant age). Note increasing BOLD signal vs. participant age while relative CBF change remains constant with age. This is driven by relatively constant $\%\Delta CMRO_2$ change with age (bottom left), and increasing *n* with age (bottom right). Values of *n* plotted are median (solid line) and 95% confidence intervals (error bars) obtained from bootstrapping (1,000 iterations, resampling with replacement) of a linear fit of participant age to CBF and relative $\Delta CMRO_2$. (Error bars are much larger at older ages due to the lower values of $\Delta CMRO_2$.)

cases are developmental disorders in which signs of micropathology indirectly implicate the vasculature. For example, microscopic scarring surrounding blood vessels has been reported in autopsied cases of dyslexia [Humphreys et al., 1990]. These more subtle abnormalities may signal vascular effects, but the impact of these on the measurement of BOLD signal in this population is unknown.

We hypothesize that astrocytes (glial cells whose processes ensheath synapses, capillaries, and neuronal perikarya) and astrocytic plasticity underlie the physiological mechanisms behind the developmental changes seen in neuronal–vascular coupling. Much evidence to date demonstrates hyperemia is in large part mediated by glutamate metabolism in astrocytes [Figley and Stroman, 2011; Koehler et al., 2009; Petzold and Murthy, 2011], which have also been shown to be involved in signaling pathways [Ben Achour and Pascual, 2012] as well as synaptic plasticity [Clarke and Barres, 2013]. During excitatory neuronal activity, perisynaptic glutamate is taken up by astrocytic processes; the specific transporter systems involved require energy supplied via glycolysis [Filosa et al., 2004]. While some of the lactate produced by glycolysis may be used by postsynaptic neurons for oxidative phosphorylation (as proposed in the astrocyte–neuron lactate shuttle hypothesis [Pellerin et al., 1998]), lactate is also a mediator of hyperemia, as shown by in vivo experiments [Lin et al., 2010].

There are also additional metabolic pathways resulting in glycolysis-mediated vasodilation [Stobart and Anderson, 2013].

A straightforward explanation for changing neuronal–vascular coupling, therefore, is an increased or decreased number of astrocytic processes contacting synapses. Indeed the concept of the "tripartite synapse" is now mainstream in neuroscience [Araque et al., 1999; Oberheim et al., 2006], with about half of synapses contacted by astrocytes [Ventura and Harris, 1999]. More processes contacting synapses will result in increased glutamate uptake, a greater amount of glycolysis and/or glycogenolysis, and therefore, a greater amount of lactate and contributions from other metabolic pathways contributing to greater vasodilation. This explanation also is consistent with our findings of inverse correlation between neuronal activity and neuronal–vascular coupling. If neuronal density does not correlate with astrocytic density, then the number of astrocytes and astrocytic processes per neuron will decrease with increasing neuronal density. A conceivable alternative explanation for changing neuronal–astrocyte coupling with age is a changing number of "footplate" astrocytic processes contacting capillaries, as has been seen in mood disorders [Rajkowska et al., 2013].

Convergent evidence also demonstrates astrocytes function as more than simple supporting cells and play an active role in brain development. Bidirectional connectivity between neurons and astrocytes has been demonstrated [Araque, 2008] as astrocyte Ca^{2+} elevations can trigger the release of gliotransmitters, which modulate neuronal activity as well as synaptic transmission and plasticity. Accordingly, astrocytic glycogenolysis and astrocyte–neuron lactate transfer has been shown to be necessary for synaptic plasticity and long-term potentiation [Suzuki et al., 2011]. Additionally, astrocytic contact with synapses has been shown to be experience-dependent in rats reared in a complex environment [Jones and Greenough, 1996], especially in cortical layer IV. Thus, our results suggest that in addition to developing neuronal activity and connectivity, astrocytes and astrocytic processes may play a key role in functional brain development in children.

As discussed earlier, our results are subject to the important confound that n, which we have accurately renamed the neuralglial–vascular coupling constant, is only an approximation for the neuronal–vascular coupling constant, as baseline $CMRO_2$ is not solely due to neuronal activity. Astrocytic oxidative metabolism is estimated to account for approximately 15%–30% of total oxidative metabolism in the brain [Hertz et al., 2007]. Conceivably, this confound could substantially affect our results. If baseline astrocytic oxidative metabolism is 30% of total baseline oxidative metabolism (assuming no task-related increase in astrocytic oxidative metabolism), the neuronal $CMRO_2$ relative change will be underestimated by a factor of approximately 1.86 (due to the error of equating baseline neuronal $CMRO_2$ with baseline total $CMRO_2$), and thus n (neuralglial–vascular coupling) will overestimate the true neuronal–vascular coupling by a factor of approximately 1.86. We, therefore, cannot rule out the possibility that some of the age-related changes seen in our data may be partly driven by age-related changes in baseline astrocytic oxidative metabolism (for which there is currently no data available, since estimation of astrocytic oxidative metabolism requires the use of invasive tracers such as labeled acetate [Wyss et al., 2011] unsuitable for use in a healthy pediatric population).

However, we do not think this confound appreciably affects the conclusions, we are drawing from our study for the following reasons. In the first place, under task conditions, while the majority of the increased energy demand in astrocytes is met through glycolysis, a significant portion of the increased energy demand has been empirically shown to be also met through oxidative phosphorylation [Cruz et al., 2005; Ivanov et al., 2014; Wyss et al., 2008]. If the relative increase in astrocytic oxidative metabolism is sufficiently large to approximate the relative increase in neuronal oxidative metabolism, n will have much less bias as an estimator of neuronal–vascular coupling. More importantly, as we are hypothesizing an increased number of astrocytic processes contacting synapses with age, we would expect an age-related increase in baseline astrocytic oxidative metabolism relative to total oxidative metabolism, as the fraction of astrocytic oxidative metabolism to total oxidative metabolism has been shown to closely mirror the volume fraction of astrocytes [Hertz et al., 2007]. This effect, however, would only serve to cause a further spurious increase in BOLD signal with age unrelated to neuronal activity, as [cf. Eq. (3)] in addition to the increased blood flow ($\Delta CBF/CBF$) caused by the greater number of astrocytes, the relative change in oxygen metabolism ($\Delta CMRO_2/CMRO_{20}$) will decrease (as the denominator is larger due to the greater astrocytic metabolism).

The main limitation of the study is that we were unable to control for possible age-related changes in the calibration constant M (maximum BOLD signal) in Eqs. (1) and (3). The age-related changes found in the BOLD–CBF relationship in Analysis 1 could, in theory, could be caused by increases in M as well as increases in n. Also, for Analysis 2, we needed to assume that M varied minimally with age (although regional variability was accounted for) to relate changes in BOLD–CBF ratio to relative $CMRO_2$. We note, however, that despite this potential limitation, our conclusion about the danger of misinterpreting results in developmental BOLD studies remains valid, as possible age-related changes in M constitute yet another confound which could result in changes in BOLD signal unrelated to neuronal activity. (We were also unable to control for possible age-related changes in α, for which there is currently very limited data available.)

However, previous research summarized below indicates that (1) the magnitude of possible age-related changes in M ($\sim$5–10%) is at least one order of magnitude less than those seen in relative $\Delta CMRO_2$ or n, which change over the age range studied by approximately a factor of 2 (Figs. 5 and 7); and (2) the direction of age-related

changes in M is negative, thus controlling for them would only serve to increase the significance of our findings of increased n and decreased relative $\Delta CMRO_2$. M is a function of baseline hematocrit (Hct), cerebral blood volume (CBV_0), and oxygen extraction fraction (OEF_0), as well as other participant-independent parameters such as main magnetic field strength and MRI TE [Chiarelli et al., 2007]:

$$M = A \times TE \times CBV_0 \times [dHb_0]^{\beta} = A \times TE \times CBV_0 \times [Hct \times OEF_0]^{\beta} \quad (4)$$

where A is a constant related to the main magnetic field strength and the susceptibility difference between blood and tissue, and dHb_0 is the baseline deoxyhemoglobin concentration. Hematocrit increases by approximately 10%–15% during the developmental period [Orkin et al., 2009; Zierk et al., 2013]. However, baseline OEF decreases by approximately the same proportion [Takahashi et al., 1999]. Baseline CBV is related to baseline CBF values via a power law (Grubb's Equation [Grubb et al., 1974]), with the exponent [α in Eqs. (1) and (3)] much less than 1 [Chen and Pike, 2009; Grubb et al., 1974; Leung et al., 2009]. Since baseline CBF shows a decrease with age [Biagi et al., 2007] in gray matter of approximately 20%–30%, age-related changes in baseline CBV are expected to be approximately 5%–10% or less. Putting this all together, we expect a slight decrease in M over the developmental period of approximately 5%–10% or less.

Assuming age-related changes in M do not represent a significant confound, our approach, therefore, enabled us to investigate age-related changes in n and relative $\Delta CMRO_2$ without knowledge of the actual value of M in a noncircular manner. This approach was taken as the focus of this study was to investigate whether developmental changes in neuronal–vascular coupling may represent a significant confound in developmental BOLD fMRI studies. However, a limitation of this approach is that estimation of the actual values of n and $\Delta CMRO_2$ is not possible without circularly assuming an average value of n (as was done in Figs. 5 and 7 for illustrative purposes), which will be a subject for future research.

Future studies could incorporate a calibrated fMRI experiment [Blockley et al., 2013; Hoge, 2012] involving a hypercapnic challenge [Davis et al., 1998], hyperoxic challenge [Chiarelli et al., 2007], carbogen (combined CO_2 and O_2) challenge [Gauthier et al., 2011], or breath-hold experiment [Bulte et al., 2009], allowing direct estimation of M. However, there are specific challenges in the application of these techniques in pediatric populations. Alternatively, another modality may be used such as near-infrared spectroscopy (NIRS), which allows the direct measurement of OEF. These types of studies would allow a more direct relation of changes in BOLD–CBF coupling to changes in neuronal–vascular coupling and neuronal activity. The limitation of NIRS for in vivo applications is that penetration of the near infrared light is typically limited to less than 1 cm of the brain, precluding whole brain mapping. Future ASL/BOLD studies involving multiple tasks activating the same region could also investigate whether age-related changes in neuronal–vascular coupling are task-dependent, arising from different neuronal inputs.

Another possible further limitation is that results could be conceivably affected by transit time effects (the time it takes for blood to traverse from the tagging region into the arterial vascular compartment and then into the capillaries). As the relevant parameter estimated by the ASL scans is the relative change in CBF between baseline and active conditions [cf. Eqs. (1) and (3)], our measurements are unaffected by population differences in baseline (absolute) CBF, or in parameters used to estimate absolute CBF, such as labeling efficiency and T1 of gray matter and T1 of arterial blood, as they cancel out when calculating the relative change. The transit time, however, decreases during neuronal activity [Gonzalez-At et al., 2000; Qiu et al., 2010], affecting the measured CBF change, and the magnitude of this effect could vary with age. However, accounting for possible transit time effects would only serve to increase the magnitude of the age-related changes in n and $CMRO_2$ seen in the present study (see Appendix for details).

CONCLUSION

In conclusion, significant age-related increases in the ratio of BOLD signal to relative CBF change were found in children ages 3–18 performing a narrative comprehension task. These findings suggest the need for caution in interpreting BOLD signal changes over development as indicative of changes in neuronal activity, and suggest a key role for astrocytes and astrocytic plasticity in the developing brain.

APPENDIX

Derivation of Eqs. (1) and (3)

An empirically validated model [Davis et al., 1998; Griffeth and Buxton, 2011] relating metabolism, CBF, and BOLD signal is given as:

$$BOLD = M\left(1 - \left(\frac{CBF}{CBF_0}\right)^{\alpha-\beta}\left(\frac{CMRO_2}{CMRO_{20}}\right)^{\beta}\right)$$

While the neuronal coupling constant n relates CBF to CMRO2 changes via

$$n = \frac{\frac{CBF - CBF_0}{CBF_0}}{\frac{CMRO_2 - CMRO_{20}}{CMRO_{20}}} = \frac{\frac{\Delta CBF}{CBF_0}}{\frac{\Delta CMRO_2}{CMRO_{20}}}$$

Since

$$\frac{CBF_0}{CBF} = 1 - \frac{\Delta CBF}{CBF}$$

and

$$\frac{\frac{\mathrm{CMRO_2}}{\mathrm{CMRO_{20}}}}{\frac{\mathrm{CBF}}{\mathrm{CBF_0}}}=\frac{1+n^{-1}\frac{\Delta\mathrm{CBF}}{\mathrm{CBF_0}}}{\frac{\mathrm{CBF}}{\mathrm{CBF_0}}}=\frac{\mathrm{CBF_0}}{\mathrm{CBF}}+n^{-1}\frac{\Delta\mathrm{CBF}}{\mathrm{CBF}}=1+(n^{-1}-1)\frac{\Delta\mathrm{CBF}}{\mathrm{CBF}}$$

We have

$$\mathrm{BOLD}=M\left(1-\left(1+(n^{-1}-1)\frac{\Delta\mathrm{CBF}}{\mathrm{CBF}}\right)^{\beta}\left(1-\frac{\Delta\mathrm{CBF}}{\mathrm{CBF}}\right)^{-\alpha}\right)$$

which is approximately linear in ΔCBF/CBF. A first-order Taylor expansion in ΔCBF/CBF yields

$$\mathrm{BOLD}\approx M\left(\beta-\alpha-\beta n^{-1}\right)\frac{\Delta\mathrm{CBF}}{\mathrm{CBF}}$$

which reduces to the result in Griffeth et al. [2013] for the special case of $\beta=1$.

Since

$$n^{-1}\frac{\Delta\mathrm{CBF}}{\mathrm{CBF}}=\frac{\frac{\Delta\mathrm{CMRO_2}}{\mathrm{CMRO_{20}}}}{\frac{\Delta\mathrm{CBF}}{\mathrm{CBF_0}}}\frac{\Delta\mathrm{CBF}}{\mathrm{CBF}}=\frac{\Delta\mathrm{CMRO_2}}{\mathrm{CMRO_{20}}}\frac{\mathrm{CBF_0}}{\mathrm{CBF}}$$
$$=\frac{\Delta\mathrm{CMRO_2}}{\mathrm{CMRO_{20}}}\left(1-\frac{\Delta\mathrm{CBF}}{\mathrm{CBF}}\right)$$

Substitution yields

$$\mathrm{BOLD}\approx M(\beta-\alpha)\frac{\Delta\mathrm{CBF}}{\mathrm{CBF}}-M\beta\frac{\Delta\mathrm{CMRO_2}}{\mathrm{CMRO_{20}}}\left(1-\frac{\Delta\mathrm{CBF}}{\mathrm{CBF}}\right)$$

Analysis of Possible Transit Time Effects

In ASL imaging, CBF is estimated by comparing signal intensities between two sets of images, obtained with and without spin labeling. The two-compartment model [Wang et al., 2002] yields the following expression for relative signal change between the labeled and unlabeled acquisitions:

$$\frac{\Delta M}{M_0}=\frac{-2f\alpha}{\lambda}\left(\begin{array}{l}\left(\frac{e^{-\delta R_{1a}}}{R_{1app}}\right)\left(e^{R_{1app}\min(\delta-w,0)}-e^{R_{1app}(\delta-\tau-w)}\right)+\\ \\ \left(\frac{1}{R_{1a}}\right)\left(e^{R_{1a}(\min(\delta_a-w,0)-\delta_a)}-e^{R_{1a}(\min(\delta-w,0)-\delta)}\right)\end{array}\right),$$
$$\tau+w>\delta$$
$$\frac{\Delta M}{M_0}=\frac{-2f\alpha}{\lambda R_{1a}}\left(e^{R_{1a}(\min(\delta_a-w,0)-\delta_a)}-e^{-R_{1a}(\tau+w)}\right),\ \tau+w<\delta$$

where f is blood flow, α is labeling efficiency, λ is the blood–brain partition coefficient, R_{1a} is the R_1 of arterial blood, R_{1app} is the R_1 of gray matter, τ is the labeling duration, w is the postlabel delay, δ is the tissue transit time (time for the labeled spins to transit from the labeling plane into the capillaries), δ_a is the arterial transit time (time for the labeled spins to transit from the labeling plane into the arterial vascular compartment).

During a functional ASL acquisition, pairs of labeled and nonlabeled acquisitions are obtained both during the baseline condition and during the task condition. All parameters in the above expression remain constant between the baseline and task conditions except for blood flow and transit times. Ideally, transit times would also remain the same, making the relative change in blood flow equal to the relative change in $\Delta M/M_0$.

However, both arterial and tissue transit times have been shown to be shorter under neuronal activity [Gonzalez-At et al., 2000; Qiu et al., 2010], causing the measured $\Delta M/M_0$ to be different than the actual relative change in blood flow. The transit times are shorter since the average blood velocity is faster as CBV does not scale linearly with CBF but rather is related via a power law. Since

$\frac{\mathrm{CBF}}{\mathrm{CBF_0}}\approx\frac{\mathrm{CBV}}{\mathrm{CBV_0}}\frac{\bar{v}}{\bar{v}_0}$ where $\bar{v}$and $\bar{v}_0$are the average blood velocities under the task and baseline conditions, respectively, and $\left(\frac{\mathrm{CBF}}{\mathrm{CBF_0}}\right)^{\alpha}\approx\frac{\mathrm{CBV}}{\mathrm{CBV_0}}$ (Grubb's relation)

$\left(\frac{\mathrm{CBF}}{\mathrm{CBF_0}}\right)^{1-\alpha}\approx\frac{\bar{v}}{\bar{v}_0}\approx\frac{\delta_{a0}}{\delta_a}\approx\frac{\delta_0}{\delta}$ where are tissue (arterial) transit times in the task and baseline conditions, respectively.

For our simulation, we used literature values of $f=60$ ml/100 g/min, $T_{1a}=1{,}660$ ms, $T_{1app}=1{,}300$ ms, $\lambda=0.9$ ml blood/g brain, α (labeling efficiency) = 0.8 [Schmithorst et al., 2014]; as values for transit times vary somewhat in the literature due to regional variability and different estimation techniques we used the "worst-case" scenario of long transit times of $\delta_{a0}=940$ ms and $\delta_0=1{,}900$ ms [Liu et al., 2011], α (Grubb's coefficient) = 0.35 [Grubb et al., 1974]. We used the values of $\tau=1{,}500$ ms and $w=800$ ms used in our ASL/BOLD acquisitions (the value of w is estimated for the lowest level of changes of BOLD–CBF coupling as shown in Figure 1; it is slightly higher than the nominal $w=700$ ms due to time necessary to acquire data from lower slices.) We then simulated measured $\mathrm{CBF/CBF_0}$ as a function of actual $\mathrm{CBF/CBF_0}$. We repeated the simulation for shorter values of δ_0 and δ_{a0} as CBF is higher in the youngest children in our age range by approximately a ratio of 1.4/1 [Biagi et al., 2007], resulting in transit times approximately 80% of the adult values from the above equation.

The simulations revealed a substantial overestimation of the true CBF in the older age group but not in the younger age group, as these shorter transit times are in the regime where the postlabel delay is larger than the arterial transit time. As lower relative CBF changes at older ages would result in a lower relative $\mathrm{CMRO_2}$ change and a higher n, increasing the strength of our found correlations with age, we can conclude that transit time effects may be hindering the sensitivity of our analyses but are not a confounding factor in interpretation of our results.

ACKNOWLEDGMENTS

The authors would like to thank Jessica Wisnowski, Ph.D., for helpful discussion on earlier drafts of this manuscript.

REFERENCES

Aguirre GK, Detre JA, Zarahn E, Alsop DC (2002): Experimental design and the relative sensitivity of BOLD and perfusion fMRI. Neuroimage 15:488–500.

Araque A (2008): Astrocytes process synaptic information. Neuron Glia Biol 4:3–10.

Araque A, Parpura V, Sanzgiri RP, Haydon PG (1999): Tripartite synapses: glia, the unacknowledged partner. Trends Neurosci 22:208–215.

Avants BB, Epstein CL, Grossman M, Gee JC (2008): Symmetric diffeomorphic image registration with cross-correlation: evaluating automated labeling of elderly and neurodegenerative brain. Med Image Anal 12:26–41.

Ben Achour S, Pascual O (2012): Astrocyte-neuron communication: functional consequences. Neurochem Res 37:2464–2473.

Biagi L, Abbruzzese A, Bianchi MC, Alsop DC, Del Guerra A, Tosetti M (2007): Age dependence of cerebral perfusion assessed by magnetic resonance continuous arterial spin labeling. J Magn Reson Imaging 25:696–702.

Blockley NP, Griffeth VE, Simon AB, Buxton RB (2013): A review of calibrated blood oxygenation level-dependent (BOLD) methods for the measurement of task-induced changes in brain oxygen metabolism. NMR Biomed 26:987–1003.

Bulte DP, Drescher K, Jezzard P (2009): Comparison of hypercapnia-based calibration techniques for measurement of cerebral oxygen metabolism with MRI. Magn Reson Med 61:391–398.

Chen JJ, Pike GB (2009): BOLD-specific cerebral blood volume and blood flow changes during neuronal activation in humans. NMR Biomed 22:1054–1062.

Chiarelli PA, Bulte DP, Wise R, Gallichan D, Jezzard P (2007): A calibration method for quantitative BOLD fMRI based on hyperoxia. Neuroimage 37:808–820.

Church JA, Petersen SE, Schlaggar BL (2010): The "Task B problem" and other considerations in developmental functional neuroimaging. Hum Brain Mapp 31:852–862.

Church JA, Petersen SE, Schlaggar BL (2012): Comment on "The physiology of developmental changes in BOLD functional imaging signals" by Harris, Reynell, and Attwell. Dev Cogn Neurosci 2:220–222.

Clarke LE, Barres BA (2013): Emerging roles of astrocytes in neural circuit development. Nat Rev Neurosci 14:311–321.

Cruz NF, Lasater A, Zielke HR, Dienel GA (2005): Activation of astrocytes in brain of conscious rats during acoustic stimulation: acetate utilization in working brain. J Neurochem 92:934–947.

Davis TL, Kwong KK, Weisskoff RM, Rosen BR (1998): Calibrated functional MRI: mapping the dynamics of oxidative metabolism. Proc Natl Acad Sci USA 95:1834–1839.

Dosenbach NU, Nardos B, Cohen AL, Fair DA, Power JD, Church JA, Nelson SM, Wig GS, Vogel AC, Lessov-Schlaggar CN, Dubis JW, Feczko E, Coalson RS, Pruett JR, Jr, Barch DM, Petersen SE, Schlaggar BL (2010): Prediction of individual brain maturity using fMRI. Science 329:1358–1361.

Fernandez-Seara MA, Aznarez-Sanado M, Mengual E, Loayza FR, Pastor MA (2009): Continuous performance of a novel motor sequence leads to highly correlated striatal and hippocampal perfusion increases. Neuroimage 47:1797–1808.

Figley CR, Stroman PW (2011): The role(s) of astrocytes and astrocyte activity in neurometabolism, neurovascular coupling, and the production of functional neuroimaging signals. Eur J Neurosci 33:577–588.

Filosa JA, Bonev AD, Nelson MT (2004): Calcium dynamics in cortical astrocytes and arterioles during neurovascular coupling. Circ Res 95:e73–e81.

Gauthier CJ, Madjar C, Tancredi FB, Stefanovic B, Hoge RD (2011): Elimination of visually evoked BOLD responses during carbogen inhalation: implications for calibrated MRI. Neuroimage 54:1001–1011.

Gonzalez-At JB, Alsop DC, Detre JA (2000): Cerebral perfusion and arterial transit time changes during task activation determined with continuous arterial spin labeling. Magn Reson Med 43:739–746.

Greve DN, Fischl B (2009): Accurate and robust brain image alignment using boundary-based registration. Neuroimage 48:63–72.

Griffeth VE, Buxton RB (2011): A theoretical framework for estimating cerebral oxygen metabolism changes using the calibrated-BOLD method: modeling the effects of blood volume distribution, hematocrit, oxygen extraction fraction, and tissue signal properties on the BOLD signal. Neuroimage 58: 198–212.

Griffeth VE, Blockley NP, Simon AB, Buxton RB (2013): A New functional MRI approach for investigating modulations of brain oxygen metabolism. PLoS One 8:e68122.

Grubb RL, Jr, Raichle ME, Eichling JO, Ter-Pogossian MM (1974): The effects of changes in $PaCO_2$ on cerebral blood volume, blood flow, and vascular mean transit time. Stroke 5:630–639.

Harris JJ, Reynell C, Attwell D (2011): The physiology of developmental changes in BOLD functional imaging signals. Dev Cogn Neurosci 1:199–216.

Hertz L, Peng L, Dienel GA (2007): Energy metabolism in astrocytes: high rate of oxidative metabolism and spatiotemporal dependence on glycolysis/glycogenolysis. J Cereb Blood Flow Metab 27:219–249.

Hoge RD (2012): Calibrated FMRI. Neuroimage 62:930–937.

Hoge RD, Atkinson J, Gill B, Crelier GR, Marrett S, Pike GB (1999): Investigation of BOLD signal dependence on cerebral blood flow and oxygen consumption: the deoxyhemoglobin dilution model. Magn Reson Med 42:849–863.

Holland SK, Vannest J, Mecoli M, Jacola LM, Tillema JM, Karunanayaka PR, Schmithorst VJ, Yuan W, Plante E, Byars AW (2007): Functional MRI of language lateralization during development in children. Int J Audiol 46:533–551.

Holland SK, Altaye M, Robertson S, Byars AW, Plante E, Szaflarski JP (2014): Data on the safety of repeated MRI in healthy children. NeuroImage: Clinical 4:526–530.

Humphreys P, Kaufmann WE, Galaburda AM (1990): Developmental dyslexia in women: neuropathological findings in three patients. Ann Neurol 28:727–738.

Hutchison JL, Shokri-Kojori E, Lu H, Rypma B (2013): A BOLD perspective on age-related neurometabolic-flow coupling and neural efficiency changes in human visual cortex. Front Psychol 4:244.

Ivanov AI, Malkov AE, Waseem T, Mukhtarov M, Buldakova S, Gubkina O, Zilberter M, Zilberter Y (2014): Glycolysis and oxidative phosphorylation in neurons and astrocytes during network activity in hippocampal slices. J Cereb Blood Flow Metab 34:397–407.

Jenkinson M, Bannister P, Brady M, Smith S (2002): Improved optimization for the robust and accurate linear registration and motion correction of brain images. Neuroimage 17:825–841.

Jenkinson M, Smith S (2001): A global optimisation method for robust affine registration of brain images. Med Image Anal 5: 143–156.

Jones TA, Greenough WT (1996): Ultrastructural evidence for increased contact between astrocytes and synapses in rats reared in a complex environment. Neurobiol Learn Mem 65: 48–56.

Kastrup A, Kruger G, Neumann-Haefelin T, Glover GH, Moseley ME (2002): Changes of cerebral blood flow, oxygenation, and oxidative metabolism during graded motor activation. Neuroimage 15:74–82.

Kim SG, Rostrup E, Larsson HB, Ogawa S, Paulson OB (1999): Determination of relative CMRO2 from CBF and BOLD changes: significant increase of oxygen consumption rate during visual stimulation. Magn Reson Med 41:1152–1161.

Koehler RC, Roman RJ, Harder DR (2009): Astrocytes and the regulation of cerebral blood flow. Trends Neurosci 32:160–169.

Ledberg A, Akerman S, Roland PE (1998): Estimation of the probabilities of 3D clusters in functional brain images. Neuroimage 8:113–128.

Leung TS, Tachtsidis I, Tisdall MM, Pritchard C, Smith M, Elwell CE (2009): Estimating a modified Grubb's exponent in healthy human brains with near infrared spectroscopy and transcranial Doppler. Physiol Meas 30:1–12.

Lim J, Wu WC, Wang J, Detre JA, Dinges DF, Rao H (2010): Imaging brain fatigue from sustained mental workload: an ASL perfusion study of the time-on-task effect. Neuroimage 49:3426–3435.

Lin AL, Gao JH, Duong TQ, Fox PT (2010): Functional neuroimaging: a physiological perspective. Front Neuroenergetics 2.

Liu P, Uh J, Lu H (2011): Determination of spin compartment in arterial spin labeling MRI. Magn Reson Med 65:120–127.

Luna B, Padmanabhan A, O'Hearn K (2010): What has fMRI told us about the development of cognitive control through adolescence? Brain Cogn 72:101–113.

Mumford JA, Hernandez-Garcia L, Lee GR, Nichols TE (2006): Estimation efficiency and statistical power in arterial spin labeling fMRI. Neuroimage 33:103–114.

Oberheim NA, Wang X, Goldman S, Nedergaard M (2006): Astrocytic complexity distinguishes the human brain. Trends Neurosci 29:547–553.

Orkin S, Fisher D, Look AT, Lux S, Ginsburg D, Nathan D. 2009. Nathan & Oski's Hematology of Infancy and Childhood. Philadelphia, PA: Saunders.

Peiying L, Andrew CH, Karen MR, Kristen MK, Jarren S, Denise CP, Hanzhang L (2013): Age-related differences in memory-encoding fMRI responses after accounting for decline in vascular reactivity. Neuroimage 78:415–425.

Pellerin L, Pellegri G, Bittar PG, Charnay Y, Bouras C, Martin JL, Stella N, Magistretti PJ (1998): Evidence supporting the existence of an activity-dependent astrocyte-neuron lactate shuttle. Dev Neurosci 20:291–299.

Petzold GC, Murthy VN (2011): Role of astrocytes in neurovascular coupling. Neuron 71:782–797.

Power JD, Barnes KA, Snyder AZ, Schlaggar BL, Petersen SE (2012): Spurious but systematic correlations in functional connectivity MRI networks arise from subject motion. Neuroimage 59:2142–2154.

Qiu M, Paul Maguire R, Arora J, Planeta-Wilson B, Weinzimmer D, Wang J, Wang Y, Kim H, Rajeevan N, Huang Y, Carson RE, Constable RT (2010): Arterial transit time effects in pulsed arterial spin labeling CBF mapping: Insight from a PET and MR study in normal human subjects. Magn Reson Med 63(2):374–384.

Rajkowska G, Hughes J, Stockmeier CA, Javier Miguel-Hidalgo J, Maciag D (2013): Coverage of blood vessels by astrocytic endfeet is reduced in major depressive disorder. Biol Psychiatry 73:613–621.

Rubinov M, Sporns O (2010): Complex network measures of brain connectivity: uses and interpretations. Neuroimage 52:1059–1069.

Schapiro MB, Schmithorst VJ, Wilke M, Byars AW, Strawsburg RH, Holland SK (2004): BOLD fMRI signal increases with age in selected brain regions in children. Neuroreport 15:2575–2578.

Schmithorst VJ, Hernandez-Garcia L, Vannest J, Rajagopal A, Lee G, Holland SK (2014): Optimized simultaneous ASL and BOLD functional imaging of the whole brain. J Magn Reson Imaging 39:1104–1117.

Smith SM (2002): Fast robust automated brain extraction. Hum Brain Mapp 17:143–155.

Stobart JL, Anderson CM (2013): Multifunctional role of astrocytes as gatekeepers of neuronal energy supply. Front Cell Neurosci 7:38.

Suzuki A, Stern SA, Bozdagi O, Huntley GW, Walker RH, Magistretti PJ, Alberini CM (2011): Astrocyte-neuron lactate transport is required for long-term memory formation. Cell 144:810–823.

Szaflarski JP, Schmithorst VJ, Altaye M, Byars AW, Ret J, Plante E, Holland SK (2006): A longitudinal functional magnetic resonance imaging study of language development in children 5 to 11 years old. Ann Neurol 59:796–807.

Szaflarski JP, Altaye M, Rajagopal A, Eaton K, Meng X, Plante E, Holland SK (2012): A 10-year longitudinal fMRI study of narrative comprehension in children and adolescents. Neuroimage 63:1188–1195.

Takahashi T, Shirane R, Sato S, Yoshimoto T (1999): Developmental changes of cerebral blood flow and oxygen metabolism in children. AJNR Am J Neuroradiol 20:917–922.

Tustison NJ, Avants BB, Cook PA, Zheng Y, Egan A, Yushkevich PA, Gee JC (2010): N4ITK: improved N3 bias correction. IEEE Trans Med Imaging 29:1310–1320.

Uludag K, Dubowitz DJ, Yoder EJ, Restom K, Liu TT, Buxton RB (2004): Coupling of cerebral blood flow and oxygen consumption during physiological activation and deactivation measured with fMRI. Neuroimage 23:148–155.

Ventura R, Harris KM (1999): Three-dimensional relationships between hippocampal synapses and astrocytes. J Neurosci 19: 6897–6906.

Wang J, Alsop DC, Li L, Listerud J, Gonzalez-At JB, Schnall MD, Detre JA (2002): Comparison of quantitative perfusion imaging using arterial spin labeling at 1.5 and 4.0 Tesla. Magn Reson Med 48:242–254.

Woolrich MW, Ripley BD, Brady M, Smith SM (2001): Temporal autocorrelation in univariate linear modeling of FMRI data. Neuroimage 14:1370–1386.

Wyss MT, Weber B, Treyer V, Heer S, Pellerin L, Magistretti PJ, Buck A (2008): Stimulation-induced increases of astrocytic oxidative metabolism in rats and humans investigated with 1–11C-acetate. J Cereb Blood Flow Metab 29:44–56.

Wyss MT, Magistretti PJ, Buck A, Weber B (2011): Labeled acetate as a marker of astrocytic metabolism. J Cereb Blood Flow Metab 31:1668–1674.

Zierk J, Arzideh F, Haeckel R, Rascher W, Rauh M, Metzler M (2013): Indirect determination of pediatric blood count reference intervals. Clin Chem Lab Med 51:863–872.

Zou P, Helton KJ, Smeltzer M, Li CS, Conklin HM, Gajjar A, Wang WC, Ware RE, Ogg RJ (2011): Hemodynamic responses to visual stimulation in children with sickle cell anemia. Brain Imaging Behav 5:295–306.